Thinning and volume loss of the Arctic Ocean sea ice cover: 2003–2008

R. Kwok,[1] G. F. Cunningham,[1] M. Wensnahan,[2] I. Rigor,[2] H. J. Zwally,[3] and D. Yi[4]

Received 2 February 2009; revised 1 April 2009; accepted 22 April 2009; published 7 July 2009.

[1] We present our best estimate of the thickness and volume of the Arctic Ocean ice cover from 10 Ice, Cloud, and land Elevation Satellite (ICESat) campaigns that span a 5-year period between 2003 and 2008. Derived ice drafts are consistently within 0.5 m of those from a submarine cruise in mid-November of 2005 and 4 years of ice draft profiles from moorings in the Chukchi and Beaufort seas. Along with a more than 42% decrease in multiyear (MY) ice coverage since 2005, there was a remarkable thinning of ~0.6 m in MY ice thickness over 4 years. In contrast, the average thickness of the seasonal ice in midwinter (~2 m), which covered more than two-thirds of the Arctic Ocean in 2007, exhibited a negligible trend. Average winter sea ice volume over the period, weighted by a loss of ~3000 km^3 between 2007 and 2008, was ~14,000 km^3. The total MY ice volume in the winter has experienced a net loss of 6300 km^3 (>40%) in the 4 years since 2005, while the first-year ice cover gained volume owing to increased overall area coverage. The overall decline in volume and thickness are explained almost entirely by changes in the MY ice cover. Combined with a large decline in MY ice coverage over this short record, there is a reversal in the volumetric and areal contributions of the two ice types to the total volume and area of the Arctic Ocean ice cover. Seasonal ice, having surpassed that of MY ice in winter area coverage and volume, became the dominant ice type. It seems that the near-zero replenishment of the MY ice cover after the summers of 2005 and 2007, an imbalance in the cycle of replenishment and ice export, has played a significant role in the loss of Arctic sea ice volume over the ICESat record.

Citation: Kwok, R., G. F. Cunningham, M. Wensnahan, I. Rigor, H. J. Zwally, and D. Yi (2009), Thinning and volume loss of the Arctic Ocean sea ice cover: 2003–2008, *J. Geophys. Res.*, *114*, C07005, doi:10.1029/2009JC005312.

1. Introduction

[2] The sea ice extent of the Northern Hemisphere has been declining at an average rate of ~3% per decade over the satellite record, and the summer decline seems to be accelerating [*Comiso et al.*, 2008]. In September 2007, the summer ice extent reached a record minimum of 4.2 × 10^6 km^2, which was 1.6 × 10^6 km^2 or 23% less than the previous record set in September 2005 [*Stroeve et al.*, 2008]. The summer retreat was particularly pronounced in the East Siberian, Chukchi, and Beaufort seas. Contrary to the daily observations of ice extent available from satellite observations, there has been a lack of ice thickness data to provide a spatial picture of the basin-scale response of the ice cover to warming trends in the Arctic associated with changes in the atmosphere [*Rigor and Wallace*, 2004] and the ocean [*Woodgate et al.*, 2006; *Polyakov et al.*, 2007]. Very little ice draft data are available from submarine cruises for the period after the concerted Scientific Ice Explorations (SCICEX) efforts of the 1990s, and this paucity of ice draft data has become especially acute. The most current publication documenting the decline in Arctic sea ice thickness [*Rothrock et al.*, 2008], based on ice draft profiles from submarine transects, covers only the period between 1975 and 2000. In view of the rapid changes of the ice extent during the past 5 years, there is a compelling need for up-to-date spatial patterns of Arctic sea ice thickness. The focus of the present note is the use Ice, Cloud, and land Elevation Satellite (ICESat) data to address this need.

[3] Recent papers [*Kwok et al.*, 2004, 2006, 2007; *Forsberg and Skourup*, 2005; *Zwally et al.*, 2008; *Kwok and Cunningham*, 2008] have demonstrated the feasibility of retrieving freeboard and ice thickness from ICESat data. In particular, comparison of the mean ice drafts from two ICESat campaigns with those from moorings in the Beaufort Sea shows relative agreement to within 0.5 m [*Kwok and Cunningham*, 2008] (henceforth KC08). In this paper,

[1]Jet Propulsion Laboratory, California Institute of Technology, Pasadena, California, USA.
[2]Polar Science Center, Applied Physics Laboratory, University of Washington, Seattle, Washington, USA.
[3]Cryospheric Sciences Branch, NASA Goddard Space Flight Center, Greenbelt, Maryland, USA.
[4]SGT, Inc., NASA Goddard Space Flight Center, Greenbelt, Maryland, USA.

Copyright 2009 by the American Geophysical Union.
0148-0227/09/2009JC005312

we use the procedures described in KC08 to convert the sea ice elevation profiles from the ICESat lidar to estimates of ice thickness. Since its launch in January of 2003 [*Zwally et al.*, 2002], ICESat has been acquiring elevation data over the Arctic Ocean with its laser altimeter which has a ~70 m footprint. With an orbit inclination of 94°, the Arctic Ocean is covered to 86°N. To date, the mission has completed 14 operational campaigns providing a 6-year record of global observations from 2003 to present. In this paper, we present our best estimate of the thickness and volume of the Arctic Ocean ice cover from 10 ICESat campaigns that span a 5-year period between 2004 and 2008. This paper (1) describes an additional improvement in the ice thickness estimation procedure, (2) provides a more extensive assessment of the derived ice thickness, and (3) summarizes the changes in the Arctic Ocean sea ice thickness and volume over the ICESat record to date.

[4] The paper is organized as follows. Section 2 describes the ICESat products and ancillary data sets used in our analyses. A brief summary of the procedures used to convert ICESat freeboard to estimates of sea ice thickness is provided in section 3. An adjustment of the freeboard to compensate for the elevation biases due to sea surface references (areas) that do not completely fill the laser footprint has been added. Section 4 describes the results from our assessment of ICESat-derived thickness using ice draft profiles from a SCICEX submarine cruise in mid-November of 2005, and 4 years of ice draft profiles from moorings in the Chukchi and Beaufort seas. The seasonal variability of the Arctic Ocean sea ice freeboard, snow depth, thickness, and volume from the 10 ICESat campaigns are discussed in section 5. Trends in these quantities are discussed in section 6. Section 7 considers the role of export and melt in the decline in ice thickness and volume over the record. Section 8 presents conclusions. For the reader interested only in the changes in the Arctic Ocean sea ice cover in the recent ICESat record, sections 3 and 4 can be skipped.

2. Data Description

2.1. ICESat Campaigns Used

[5] Elevation data from 10 ICESat campaigns are used in this paper. Table 1 shows the laser and campaign designations, their exact dates, and the duration of each campaign. Data products are of release 428: the latest and best releases available in terms of the quality of the precision orbit and attitude determination at the time of this writing. Broadly, these 10 campaigns span a period of 5 years, and were selected to provide representative sampling of the fall and winter sea ice cover of the Arctic Ocean. Throughout this paper, we use the following campaign designations: ON03, FM04, ON04, FM05, ON05, FM06, ON06, MA07, ON07, and FM08. We note here that the campaigns start dates vary (by almost a month) even though the length of laser operation, except for ON03, remains ~34 days. For instance, the fall ON06 campaign started later in October while MA07 is the only winter campaign on the list that started in mid-March. We also note that these are not the only ICESat campaigns; these 10 were selected for examination of the interannual and seasonal variability in the retrieved freeboard, snow depth, sea ice thickness and volume over the record.

2.2. Ice Draft From Profiling Systems

2.2.1. Submarine Cruises

[6] Ice draft data from a number of submarine transects of the Arctic basin were used. The data are provided by the U.S Navy Arctic Submarine Lab and archived at the *National Snow and Ice Data Center* (NSIDC) [2006]. The data consist of first return draft measurements made every few meters with a nominal footprint size of between 2.5 and 6 m. These data are recorded either digitally or in analog form with care taken to produce equivalent data from the two recording media [*Wensnahan and Rothrock*, 2005]. This paper also uses a new data set acquired in October/November 2005 (Figure 3a) which are currently not available at NSIDC. The 2005 data are in the form of analog paper charts and were digitized using the techniques of *Wensnahan and Rothrock* [2005]. Mean draft was derived for segments of the cruise varying from 15 to 50 km in length. An assessment of the quality of the submarine draft data set can be found by *Rothrock and Wensnahan* [2007]. In general, the error in the mean is approximately 25 cm. The data are biased with respect to actual draft due to the first return nature of the product by approximately +29 ± 12 cm.

2.2.2. Fixed Mooring Sites

[7] Ice draft time series are also obtained from two sets of moorings. One set is deployed in the Canada Basin as part of the Beaufort Gyre Exploration Project (www.whoi.edu/beaufortgyre; *Proshutinsky et al.* [2004]) and the other is from one Arctic Ice Monitoring (AIM) site in the Chukchi Sea operated by the Institute of Ocean Sciences (Sidney, Canada). The Beaufort Gyre Exploration Project (BGEP) moorings have been operational since 2003. At these moorings, upward looking sonars (ASL Environmental Sciences model IPS-4) are typically located between 50 and 85 m beneath the ice cover (depending on actual mooring length and deployment depth). A directed 420-kHz beam ranges to the bottom surface of the sea ice every two seconds with a footprint of about 2 m. Seawater pressure and temperature are recorded by each instrument every forty seconds. Ice draft is determined from the corrected range minus the pressure of the transducer (corrected for atmospheric pressure variations), after taking into account instrument tilt, sound speed and density variations in the seawater. The same type of upward looking sonar is deployed at the AIM site and processed using the same procedures. In addition, the data from this site have been mapped into a pseudospatial coordinate system using ice velocities derived from an acoustic Doppler sonar. That is, ice draft profiles are presented in regular spatial increments rather than in time increments. Methods used in the processing and calibration of the sonar to yield ice draft are described by *Melling et al.* [1995]; individual ice drafts are typically accurate to within ±0.1 m (95% confidence limits).

2.3. Other Data Sets

[8] Gridded fields of multiyear (MY) ice fraction are from the analysis of QuikSCAT data [*Kwok*, 2004]. QuikSCAT is a moderate resolution wide-swath (1800 km) K_u-band

Table 1. ICESat Data Used

Laser	Campaign[a]	Period	Days of Operation
2a	ON03	24 Sep to 18 Nov	55
2b	FM04	17 Feb to 21 Mar	34
3a	ON04	3 Oct to 8 Nov	37
3b	FM05	17 Feb to 24 Mar	36
3d	ON05	21 Oct to 24 Nov	35
3e	FM06	22 Feb to 27 Mar	34
3g	ON06	25 Oct to 27 Nov	34
3h	MA07	12 Mar to 14 Apr	34
3i	ON07	2 Oct to 5 Nov	37
3j	FM08	17 Feb to 21 Mar	34

[a]Campaign notation is mmyy.

scatterometer that provides daily coverage of the Arctic Ocean at V and H polarizations with spatial resolutions of ~25 km at incidence angles of 53° and 45°. Daily ice motion fields are derived from the AMSR-E satellite passive microwave observations (89-GHz channel) using the procedures in *Kwok et al.* [1998]. Daily ice concentration fields are also from AMSR-E. The ECMWF meteorological fields are provided by the Data Support Section of the Scientific Computing Division at the National Center for Atmospheric Research (NCAR). These fields are on a Gaussian (n80) grid with a resolution of approximately 1.125°.

3. ICESat Freeboard and Thickness

[9] In this section, we provide a description of (1) the process used in the estimation of ice thickness and (2) an additional freeboard adjustment introduced to compensate for the elevation biases in freeboard when the sea surface references (areas of leads and thin ice) do not fully fill the entire laser footprint.

3.1. Freeboard to Thickness

[10] Our methods to retrieve freeboard and to estimate ice thickness are based on those in *Kwok et al.* [2007] and KC08. The reader is referred to these papers for more detailed descriptions and assessments of these approaches. Here, we outline very briefly the steps taken to obtain the fields of ice thickness from the 10 ICESat campaigns.

[11] ICESat freeboard, as used here, is the vertical elevation of the air-snow interface from the local sea surface (Figure 1). For the Arctic Ocean, the total freeboard consists generally of a snow layer superimposed on the freeboard of floating sea ice. This total freeboard height, h_f, above the sea surface can be written as the sum of two terms:

$$h_f = h_{fs} + h_{fi}, \tag{1}$$

where h_{fs} and h_{fi} are the thicknesses of the snow and ice layers above the sea surface.

[12] The total freeboard, h_f, is the difference between surface elevation, h_{obs}, as measured by a laser altimeter and the sea surface height, h_{ssh}:

$$h_f(x, t_i) = h_{obs}(x, t_i) - h_{ssh}(x, t_i). \tag{2}$$

Both h_{obs} and h_{ssh} are defined, in the case of ICESat, relative to the TOPEX/Poseidon ellipsoid.

[13] Since we lack centimeter-level knowledge of the time-variable sea surface height, a necessary step in retrieving freeboard is the identification of available sea surface references (tie points) over the ice cover. The practical issues associated with the identification of sea surface samples in ICESat data can be found in *Kwok et al.* [2007]. Briefly, our freeboard estimates (h_f) are derived by combining the sea surface elevations (h_{ssh} tie points) from three different procedures. In order of decreasing quality, these approaches select elevation samples (1) of new openings identified in ICESat profiles and SAR imagery, (2) where the ICESat reflectivities are below those of the background snow covered sea ice and where their elevations exceed an expected deviation below that of a local mean surface, and (3) where the only condition is that their elevations exceed an expected deviation below that of a local mean surface. We designate these three categories of tie points as H_{op}, $H_{\Delta R}$, and H_{σ}. The strength of the second and third approaches is that they do not depend on the availability of SAR imagery and offer a larger density of tie points to provide a more complete depiction of the spatial pattern of sea ice freeboard over the Arctic Basin. Using the tie points from new openings (H_{op}) for assessment of the second and third categories ($H_{\Delta R}$ and H_{σ}), *Kwok et al.* [2007] showed that the consistency in the identification of h_{ssh} tie points from these two approaches is ~5 cm (standard deviation). Our estimate of h_{ssh} within a 25-km segment is the weighted average of available tie points; the weights are computed on the basis of measures of their quality [*Kwok et al.*, 2007]. Overall, the results suggest that the retrieval procedures provide consistent freeboard estimates along 25-km segments (containing ~140 ICESat samples) with uncertainties of better than 7 cm (with a fraction of that due to a bias of ~3–4 cm).

[14] The retrieved sea surface heights (h_{ssh}) are then adjusted for two sources of bias: snow layer and coverage of sea surface reference (area) within lidar footprint. First, if an area of snow covered thin/new ice were identified as a tie point, the snow layer would increase the elevation of that sea surface tie point (h_{ssh}) and lead to an underestimation of freeboard (h_f). KC08 introduced a nominal adjustment for

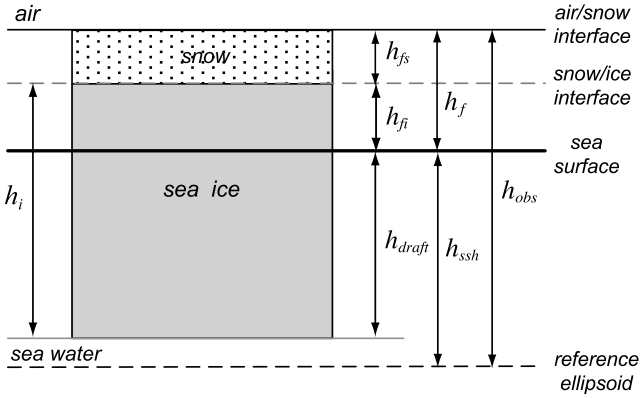

Figure 1. Schematic showing the arrangement of sea ice freeboard, draft, and thickness discussed in section 2.

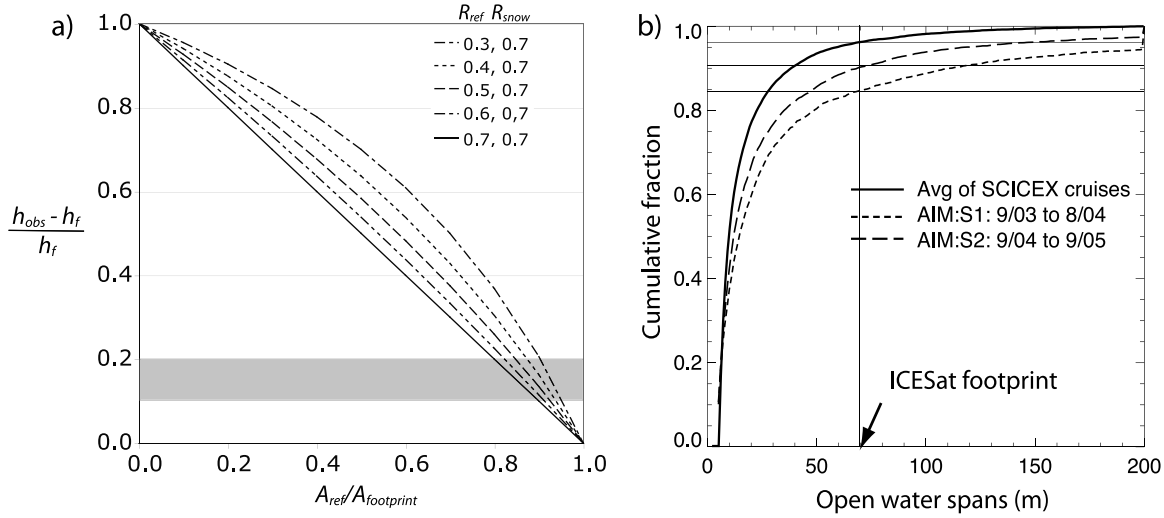

Figure 2. Freeboard error and lead "widths." (a) Dependence of freeboard error on lead reflectivity (R) and fractional coverage within the lidar footprint. (b) Cumulative distribution of the length open-water spans from Arctic Ice Monitoring (AIM) and Scientific Ice Expeditions (SCICEX) ice draft profiles. Figure 4a shows the location of AIM mooring in the Chukchi Sea. The AIM data set covers the two seasons between September 2003 and August 2004 (S1) and between September 2004 and 2005 (S2). Ice drafts from five SCICEX cruises (1993, 1996, 1997, 1998, and 1999) are used to create the average cumulative distribution (solid line). All SCICEX data, except for 1999, were acquired during the summer and fall.

snow coverage (over thin ice) based on the reflectivity of that elevation sample and have demonstrated the efficacy of that correction in reducing the relative biases between the three categories of tie points. A second adjustment is necessary because the ICESat elevations (from waveform fitting) represent the mean of the surface elevation distribution within the laser footprint. If the sea surface and thin ice areas do not fill the footprints, the surface relief of the neighboring ice cover will contaminate the elevation of the selected tie points (i.e., local sea surface). Thus, a mixture of surface elevations would cause an overestimation of the desired tie point elevation and consequently an underestimation of the retrieved freeboards. The compensation for this source of bias was not discussed in KC08 and is introduced below (in section 3.2).

[15] After the adjustment of the ICESat freeboards, the following relationship is used to compute the ice thickness (h_i) of elevation samples within 12.5 km of available tie points:

$$h_i = \left(\frac{\rho_w}{\rho_w - \rho_i}\right) h_f - \left(\frac{\rho_w - \rho_s}{\rho_w - \rho_i}\right) h_{fs}. \quad (3)$$

Using the assumption that the floating ice cover is in isostatic balance, the densities of ice (ρ_i), snow (ρ_s), and seawater (ρ_w) provide the appropriate scaling for hydrostatic equilibrium. In the following analyses, the density of seawater, ρ_w, is assumed to be constant (1024 kg/m^3) and the bulk density of snow, ρ_s, follows a seasonal behavior discussed in KC08. A constant ice density of 0.925 g/cm^3 is used [*Weeks and Lee*, 1958; *Schwarz and Weeks*, 1977]. The spatially varying snow depth, h_{fs}, is from the accumulation of snowfall (from ECMWF fields) by an advecting ice cover (using ice motion from AMSR-E). The construction of the daily fields of snow depth and the appropriate use of these daily fields are described in KC08.

3.2. Area of Sea Surface References Within Laser Footprint

[16] Sea ice freeboards (h_f) are measured relative to the elevation of the local sea surface (h_{ssh}) of water or thin ice in open leads. Unless the lead area fills the entire footprint of the lidar, the retrieved sea surface is biased by the elevation of the neighboring ice cover. As there is a range of lead widths in the Arctic Ocean, the extent of these biases is dependent on the fraction of the laser footprint occupied by the sea surface reference as well as its reflectivity (see Figure 2). When the lead/thin ice area is snow filled (i.e., lead reflectivity equals snow/ice reflectivity), the error in freeboard elevation is linearly related to the relative fraction of lead coverage ($A_{ref}/A_{footprint}$), where A_{ref} and $A_{footprint}$ are the areas of the sea surface reference and laser footprint, respectively. Furthermore, if a lead (or surface references) has lower reflectivity, as is expected of new openings or thin ice with a very thin layer of snow, the contribution of the darker lead area to the return waveform is reduced. Effectively, this increases the weighting of the elevation of the surrounding ice cover and therefore the freeboard errors within that footprint.

[17] While we have no knowledge of the area coverage of sea surface references within individual footprints, we can obtain an assessment of the fraction of our tie points that are expected to be biased based on lead width statistics. If the width of most of the leads on the ice cover are narrower than the footprints, then a nominal correction, even though imperfect, could reduce this source of error in the retrieved freeboards. However, we are not aware of lead width

statistics of the Arctic Ocean at this length scale (in the published literature) that we could use for comparison with the diameter of the ICESat footprint (~70 m). To be useful, the statistics must span lead widths in the range from meters to hundreds of meters. Here, instead of lead widths, we create a proxy of this statistic by computing the spans of open water (in meters) using ice draft profiles from moored and submarine ice profiling sonars (Figure 2b). This is a lead width proxy because it does not measure the shortest distance between two ice floes and these spans will typically be wider than the actual widths. All samples with ice drafts less than 10 cm are considered to be open water. Changing this detection criterion by 5 cm does not alter the results of this section. And, only spans with lengths of more than 5 m are included in the distributions owing to the limitations in spatial resolution (spot size) of the profiling sonars. These two data sets provide a fairly diverse sampling of the Arctic in terms of season and location: the AIM data set contains time series of ice draft at a fixed location in the Chukchi Sea over 2 years, while the SCICEX cruises span multiple years and two primary seasons. The ice draft profiles from the BGEP moorings are not used here because they have not been converted into a pseudospatial representation (uniform sampling in space) using acoustic Doppler data.

[18] The cumulative distributions of the length of these open-water spans from both the AIM moorings and five SCICEX cruises (Figure 2b) show that, on average, more than 80% of these spans are narrower than the footprint diameter of the ICESat lidar. These distributions show the likelihood that the retrieved freeboards are biased is high, especially when the reflectivity of that ICESat sample is low. In fact, the percentage of biased samples would be higher because our proxy measure overestimates actual lead widths. Moreover, we expect the likelihood to be even higher if we account for the fact that the altimeter footprints do not always cover the width of an entire lead (i.e., it could cover only a fraction of that lead) even though its width could be larger than the footprint. Thus, it is necessary and useful to devise a nominal correction of the ICESat freeboards prior to the steps to convert them to ice thickness. On the basis of residual biases in the retrieved freeboard after the snow adjustment (see Figure 3 in KC08), we apply the following reflectivity-dependent scaling, α, of the freeboard (h_f):

$$h_f' = \alpha h_f \quad where \qquad \alpha = 1.1 + 0.1\left(\frac{R_{snow} - R}{R_{ow}}\right). \tag{4}$$

R_{snow}, R_{ow}, and R are the reflectivities of snow, bare ice, and the ICESat sample, respectively. R_{snow} and R_{ow} are approximately 0.7 (the mean background reflectivity in the ICESat data) and 0.25 at the wavelength of the ICESat laser. Because it is a scale factor, the total adjustment (in meters) is dependent on the freeboard elevation and increases with the reflectivity difference between the ICESat sample and the background ice/snow. Qualitatively, this models the behavior of the freeboard-dependent residuals after the snow correction. Effectively, this compensates for biases in the 10–20% range as indicated by the gray region in Figure 2a. We feel that this is a crucial correction of the ICESat freeboards.

4. Comparisons With Ice Draft From Profiling Sonars

[19] In this section, ICESat ice drafts are compared with drafts from submarine and moored ice profiling sonars. ICESat thicknesses are converted to sea ice drafts (h_d) via: $h_d = h_i - (h_f - h_{fs})$ (see Figure 1).

4.1. Ice Draft From a Submarine Transect

[20] The operational period of the ON05 ICESat campaign overlaps with one cross-Arctic submarine transect in November 2005. Figure 3a shows this transect (in white): it originates north of Point Barrow, continues toward the North Pole, and terminates in the Nansen Basin. It is plotted against a background field of multiyear sea concentration derived from QuikSCAT. In terms of ice conditions, the transect first encounters a fragmented tongue of MY cover north of the Alaska coast, then runs into an area of low MY ice coverage (bluish colors) in the Canada Basin, before entering the thick MY ice pack of the central Arctic Ocean. The black curve in Figure 3b shows the submarine ice draft profile across the basin. The samples along the submarine profile are mean submarine ice draft of segments that are more than 15 km in length. The submarine data are provided as a set of disjointed ice draft profiles of varying lengths (segments) as determined by changes in course, speed or depth of the submarine. Importantly, an expected bias of 29 cm has been removed from the mean draft of each segment. After considering the relevant error sources in the estimation of ice draft from U. S. Navy submarines, *Rothrock and Wensnahan* [2007] reported that the measured submarine ice drafts are probably on average 29 cm too large and advised that this bias should be considered when comparing submarine ice drafts with other data sets.

Figure 3. Comparison of ICESat estimates with submarine ice drafts. (a) Submarine track (white) from Point Barrow to the eastern Arctic Ocean (between 12 and 20 November 2008) overlaid on the map of multiyear sea ice concentration derived from QuikSCAT. Dashed circle shows the ICESat data hole. (b) Profiles of mean submarine (black) and ICESat (blue) ice draft from segments >15 km in length. Quantities near the bottom of the plot (blue) show the number of near coincident ICESat segments (i.e., within 10 days and 25 km of the submarine track). (c–d) ICESat versus submarine ice draft distributions (IDD-1 and IDD-2) from a 400-km and 300-km span of the submarine ice draft profile shown in Figure 3b. The number of samples (N), the population mean, and the scatter about the mean (+RMS, −RMS) are shown. (e) Scatterplot shows mean ICESat and submarine ice drafts. N is the number of samples in the plot, and r is the correlation between the two quantities. The horizontal error bars show the expected 25-cm uncertainty of the submarine ice draft [*Rothrock and Wensnahan*, 2007], and the vertical error bars show the ±1 RMS deviations and the variability of the ICESat samples, respectively. (f) Mean ice motion during the 8-day submarine transect. (Contours are sea level pressure isobars; interval is 2hPa.)

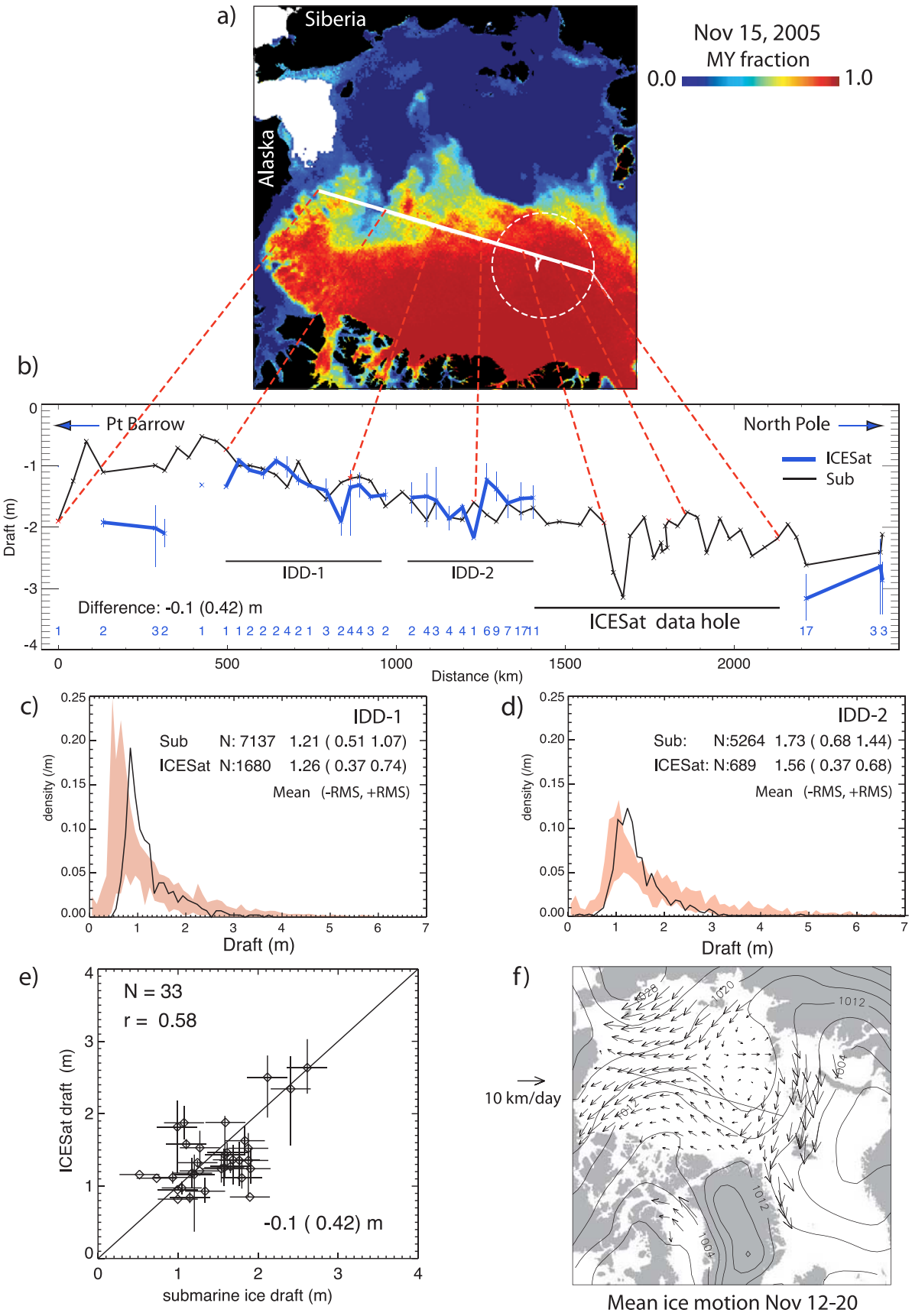
a)
Siberia
Alaska
Nov 15, 2005
MY fraction
0.0
1.0
b)
Pt Barrow
North Pole
ICESat
Sub
Draft (m)
IDD-1
IDD-2
Difference: -0.1 (0.42) m
ICESat data hole
Distance (km)
c)
IDD-1
Sub N: 7137 1.21 (0.51 1.07)
ICESat N:1680 1.26 (0.37 0.74)
Mean (-RMS, +RMS)
density (/m)
Draft (m)
d)
IDD-2
Sub: N:5264 1.73 (0.68 1.44)
ICESat: N:689 1.56 (0.37 0.68)
Mean (-RMS, +RMS)
density (/m)
Draft (m)
e)
N = 33
r = 0.58
-0.1 (0.42) m
ICESat draft (m)
submarine ice draft (m)
f)
10 km/day
Mean ice motion Nov 12-20

Figure 3

[21] For comparison with the submarine profile, we plot the mean and standard deviation of the ICESat-derived ice drafts (Figure 3b, blue) from 25-km segments that are within 5 days and 22 km of the center location of each submarine segment. Each 25-km ICESat segment contains ~140 ice draft samples. The quantities at the bottom of the plot (Figure 3b, blue) show the number of ICESat segments that satisfy our space-time proximity criteria. More ICESat segments are available at higher latitudes because of converging satellite orbits near the pole. The difference between the ICESat and submarine ice draft, after accounting for the average 29 cm bias, is −0.1 (0.42) m. The quantity in brackets is the standard deviation of the differences. Figure 3e shows the scatter of the two quantities. The horizontal error bars show the expected 25 cm uncertainty of the submarine ice draft [*Rothrock and Wensnahan*, 2007] and the vertical error bars show the ±1 RMS deviations and the variability of the ICESat samples, respectively. The thicker ICESat drafts early on in the transect stands out and could be attributed partly to the inadequate sampling of the fragmented nonuniform ice cover of MY and first-year (FY) sea ice and partly to ice advection. Near the Alaska coast, mean ice motion (Figure 3f) along the submarine transects is predominantly south at 5–6 km/day during this period. At this location, the sampling of the ice is very sensitive to the location of that tongue of thick MY ice in the southern Beaufort Sea. ICESat segments from east of the transect would sample thicker MY ice from the remnants of the summer ice cover rather than the first-year ice west of the ice cover. Past 500 km from the coast, the thickening trend across the basin seems to be in better agreement.

[22] Next, we compare the submarine and ICESat ice draft distributions (IDD) along two sections (IDD-1 and IDD-2) of the subtrack (Figures 3c and 3d). These sections are selected for the following reasons. First, they are long enough that both sample populations are large enough to provide a representative depiction of the density function. Second, they present distinctive ice conditions for assessing the sensitivity of the ICESat draft distributions. The IDD-1 section samples the thinner ice in an area of mixed MY and FY ice while IDD-2 samples the distribution in a region of thicker ice with higher MY fraction. To match the spatial resolution of the data used to construct the IDDs, the 1-m submarine ice draft samples are first averaged to form 70-m samples to mimic the diameter of the ICESat footprint. Finally, we also have to consider how to deal with the expected 29-cm bias in the submarine draft (discussed above) because just shifting the entire distribution by this amount does not seem physically reasonable as it would create negative drafts. Instead, we scale the ice draft of the two sample populations (one scale factor for each population) to obtain an effective reduction in the sample mean of 29 cm. This seems more sensible because the dominant errors are not typically introduced by the sonar measurements in the thinner end of the ice draft distribution but in the thicker end (e.g., keels of deformed ice).

[23] Figures 3c and 3d contrast the ICESat (in black) and submarine ice draft distributions (in pink). The pink envelopes show the variability of distributions along each submarine section. The mean differences in ice draft are 0.04 m and −0.17 m for the two sections. Qualitatively, it can be seen that the shapes of the two distributions are similar and that the ice is thinner in the IDD-1 section. But even though it is encouraging to see that the ICESat IDDs have fairly long tails and seem to be within the envelope of the submarine IDDs, the most distinctive feature common to both comparisons seems to be the narrower ICESat IDDs. Barring the fact that the differences could be due to space-time differences in the ICESat versus submarine IDDs, there are many factors that could contribute to the observed differences. These factors span the spectrum that covers instrumental and algorithmic issues to our understanding of the expected equivalence in the distribution of surface relief and bottom topography. The resolution of these differences, however, is quite beyond the scope of this paper.

4.2. Ice Draft From Moorings

[24] Here, we compare ice draft time series from the AIM mooring in the Chukchi Sea and from the four BGEP moorings in the Beaufort Sea with the estimates from ICESat. Figure 4a shows the location of the five moorings and the data span from each mooring.

[25] As the mooring data provide point-wise sampling of the ice draft of a moving ice field at fixed locations and the ICESat profiles provide spatial observations at essentially fixed times, an initial step is to match the spatial length scales/extent of the observations to produce comparable statistics. The mooring samples are first processed to produce twice-daily samples of the means and standard deviations of ice drafts that are representative of those from 25-km tracks. For the AIM data set, the time-sampled ice drafts have already been resampled onto a pseudospatial coordinates of 1-m spacing using the ice velocity from its acoustic Doppler sonar, and thus it is straightforward to create these 25-km statistics. Since the BGEP mooring data are provided in time-sampled format, the total number of mooring observations used in each twice-daily ice draft sample is variable; the temporal interval that covers the sample population is defined by the time it takes for the overhead ice pack to travel a net distance of ~25 km. Rough ice drift from the 89-GHz channel of AMSR-E on the Aqua platform is used in this calculation.

[26] The scatterplots (Figures 4b–4e) show the relative agreement between the ICESat and mooring ice drafts for four growth seasons: ON03/FM04, ON04/FM05, ON05/FM06, ON06/MA07. Mean ICESat-derived ice drafts are from 25-km segments that are closest in time (within half a day) and within 25 km of the moorings. The data from the fall campaigns are shown with open symbols, and the data from the winter are shown with solid symbols. The number of points that satisfy the space-time proximity criteria is small for each season. The mean differences range from −0.32 to 0.24 m, with the standard deviation of the differences at ~0.5 m for all seasons. Taken together, the overall difference is −0.14 (0.51) m with a correlation of 0.63 between the two ice draft populations (Figure 4f). The ICESat drafts tend to be biased positive in the fall and negative in winter. We do not have an explanation for this.

[27] It is interesting to note that the standard deviation of the differences is similar to that obtained from our submarine draft comparison above. The consistency of the assessment and the diversity in time and space of the mooring and submarine records give us confidence in the relative quality of the ICESat ice draft estimates. Finally, it is also important

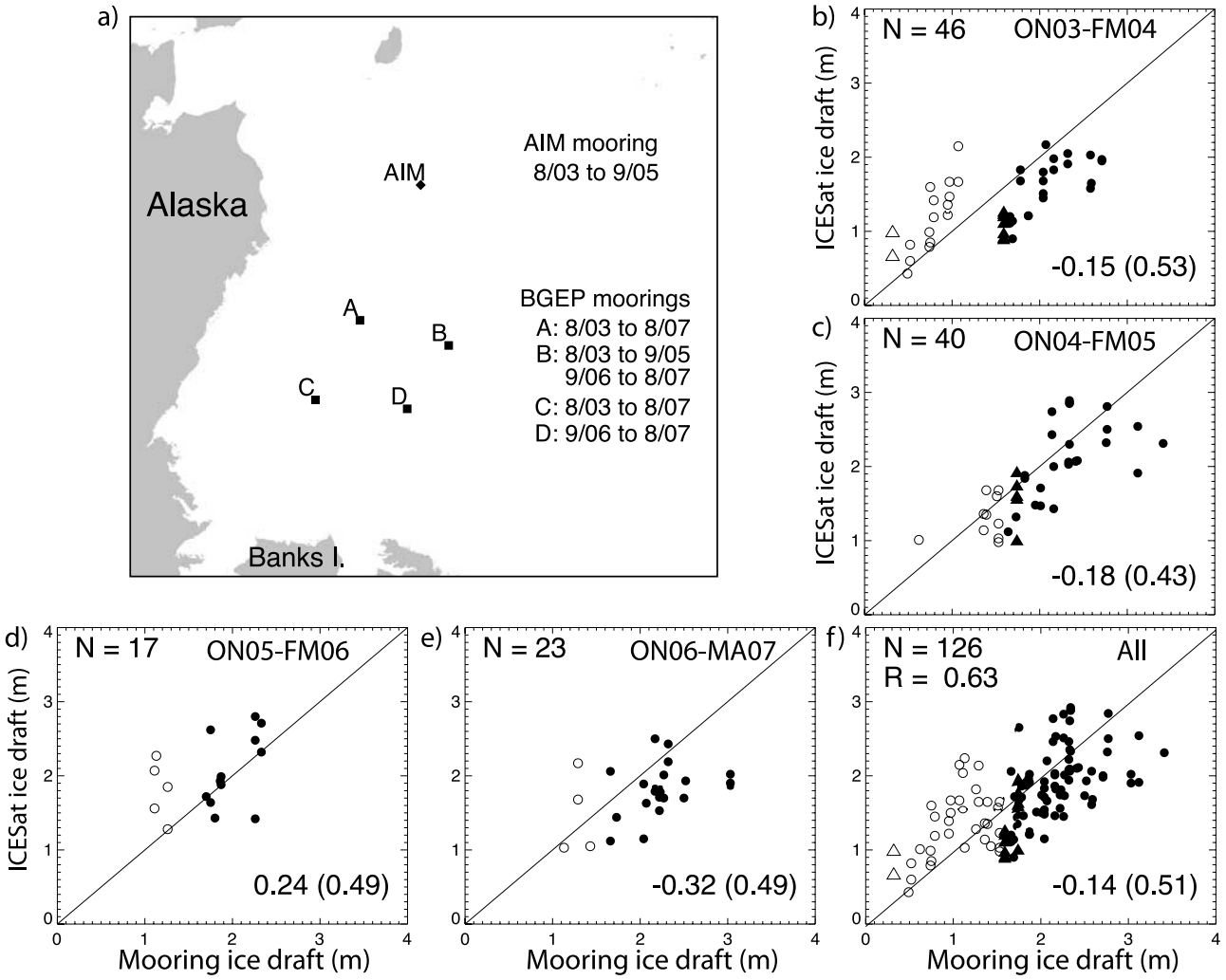

Figure 4. Comparison of ICESat estimates with ice draft from moorings. (a) Location of AIM and Beaufort Gyre Exploration Project (BGEP) moorings in the Beaufort and Chukchi seas. (b) ON03 and FM04 ICESat campaign. (c) ON04 and FM05 ICESat campaign. (d) ON05 and FM06 ICESat campaign. (e) ON06 and MA07 ICESat campaign. (f) All campaigns. (Triangles, ICESat versus AIM; circles, ICESat versus BGEP; open symbols, fall (ON campaigns); solid symbols, winter (FM and MA campaigns)). The number of samples (*N*), the correlation (*R*) between the two quantities, and the mean and standard deviation of the differences between the quantities are shown in Figures 4b–4f.

to recognize when looking at these assessments that (1) these comparisons are coincident neither in time nor space and thus variability due to these factors affects the results and (2) there are inherent uncertainties in the moored ULS ice drafts (~0.1 m). Similar to the submarine ice drafts, the moored ULS ice drafts are slightly overestimated because the sonar range represents the leading edge of the return pulse from the ice surface and would therefore be biased by keels if the spot size were large. If these factors were taken into consideration, they could reduce the differences.

5. Sea Ice Thickness and Volume: Seasonal Behavior

[28] In this section, we discuss the seasonal behavior of the freeboard, snow depth, thickness and volume of the Arctic Ocean sea ice cover during the fall and winter ICESat campaigns of 2004 through 2008. Their trends over the record are discussed in the section 6. To be specific, we refer to the Arctic Ocean as that area bounded by the gateways into the Pacific (Bering Strait), the Canadian Archipelago and the Greenland (Fram Strait) and Barents seas. Within these boundaries, the Arctic Ocean covers a fixed area of $\sim 7.2 \times 10^6$ km^2. Figure 5 shows the 5-year record of freeboard, snow depth, thickness, and volume while Figure 6 shows the detailed spatial patterns of ice thickness and their distributions. Tables 2 and 3 summarize the mean and variability of the fall and winter behavior of these four quantities. We separate the 10 ICESat campaigns into five that represent the fall (ON03, ON04, ON05, ON06, ON07) and five that represent the winter (FM04, FM05, FM06, MA07, FM08). Again, their actual start and end dates are shown in Table 1. As mentioned in section 2, the ICESat operational periods do not necessarily start at the same dates, and thus there is expected variability associated with the timing of individual campaigns for comparing their

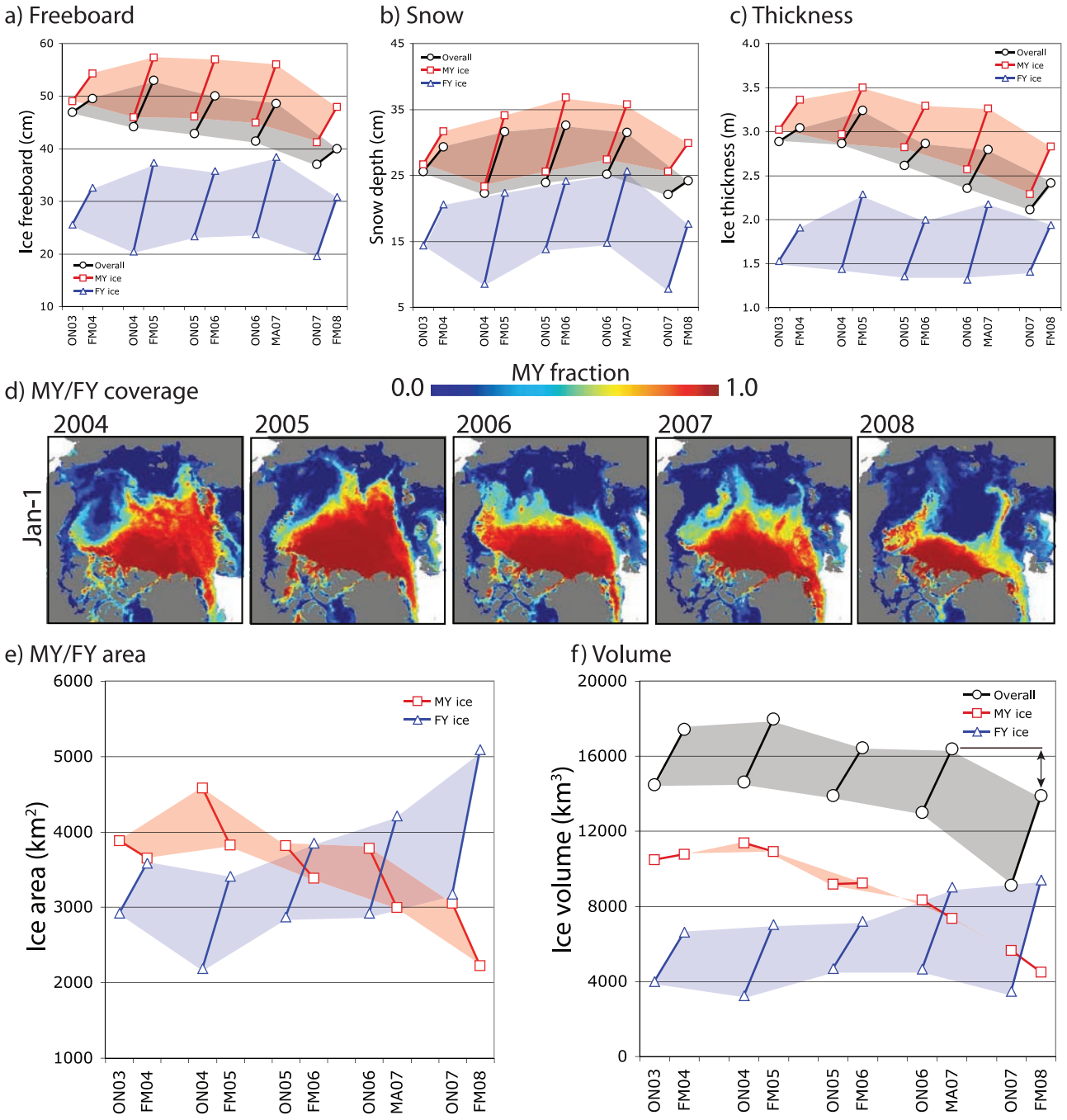

Figure 5. Changes in the Arctic Ocean sea ice freeboard, snow depth, multiyear/first-year coverage, thickness, and volume (2004–2008). (a) Freeboard. (b) Snow depth. (c) Sea ice thickness. (d) MY/FY ice coverage. (e) MY/FY ice area. (f) Ice volume. Multiyear (MY) and first-year (FY) areas are delineated using the 50% MY concentration isopleth. Uncertainties in the thickness and volume estimates are discussed in sections 5.1 and 5.2.

seasonal and interannual behavior. Typically, there is a ~4–5 month separation between the fall and winter campaigns.

[29] These quantities are also computed in regions with predominantly multiyear ice (MY fraction > 0.5) and first-year ice (MY fraction < 0.5). This partition allows us to examine the differences in their seasonal behavior associated with their age, thickness, and volume. Henceforth, we refer to these two areas as the MY and FY ice zones, respectively. The fields of MY fractions (shown in Figure 5d) used in these calculations are derived from QuikSCAT backscatter [*Kwok*, 2004].

5.1. Freeboard, Snow Depth, and Ice Thickness

[30] Figures 5a and 5b show the 5-year record of overall mean ICESat freeboard and snow depth from which the sea ice thicknesses are derived. The spatial fields are not shown here and the reader is referred to KC08 for a more detailed

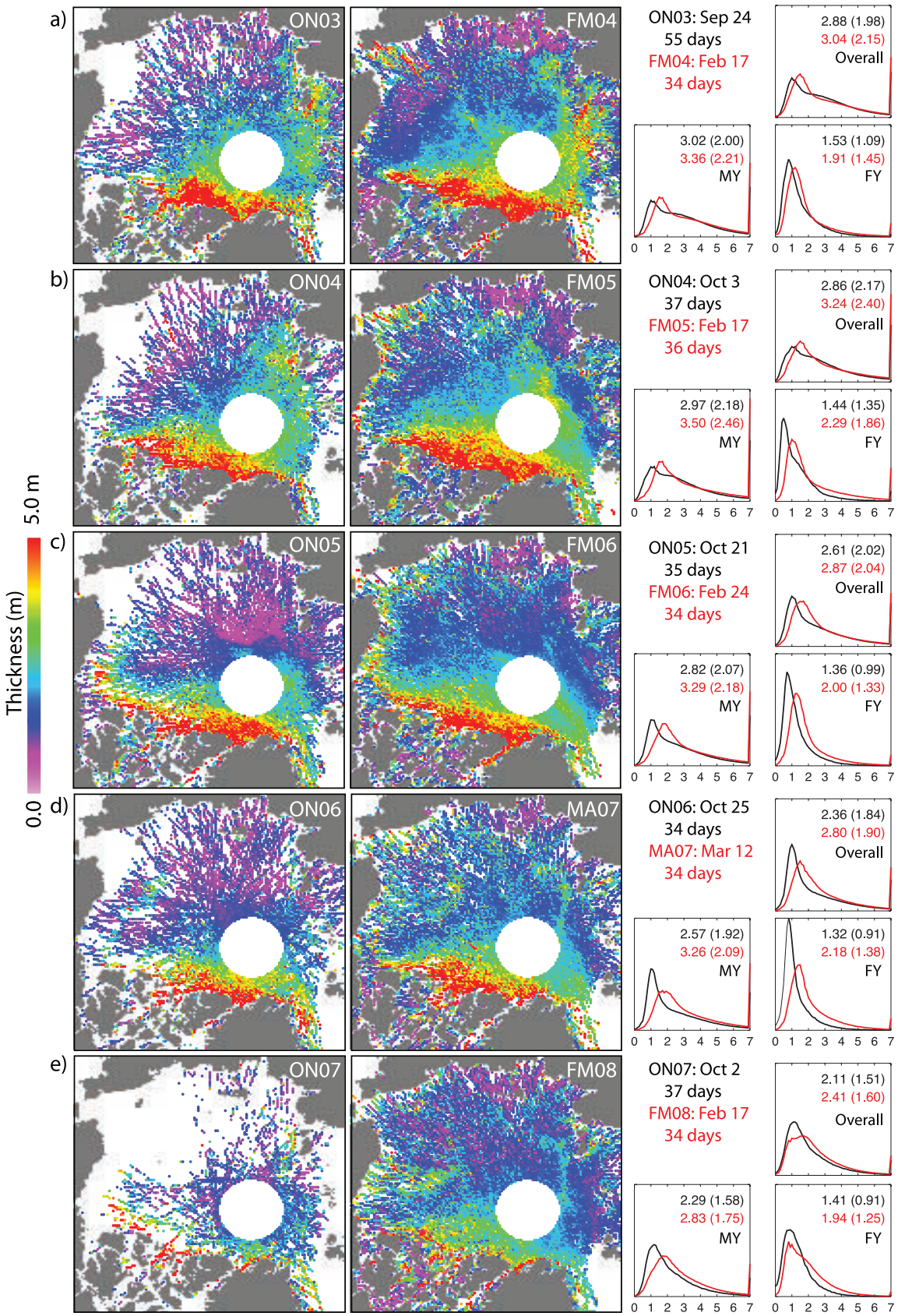

Figure 6. Sea ice thickness: Spatial patterns and their distributions. (a) ON03 and FM04. (b) ON04 and FM05. (c) ON05 and FM06. (d) ON06 and MA07. (e) ON07 and FM08. ON distributions and FM/MA distributions are plotted in black and red, respectively. MY and FY areas are delineated using the 50% MY concentration isopleth.

Table 2. Means and Trends in Sea Ice Coverage, Freeboard, Snow Depth, Thickness, and Volume During the Fall and Winter ICESat Campaigns[a]

	Overall	Overall Trend (a^{-1})	FY Ice	FY Ice Trend (a^{-1})	MY Ice	MY Ice Trend (a^{-1})
Coverage (10^3 km^2)						
1 Jan	7205 (18)	−7	3870 (581)	319	3334 (575)	−324
Ice freeboard (cm)						
Fall	42.5 (3.7)	−2.2	22.6 (2.5)	−0.9	45.5 (2.8)	−1.7
Winter	48.2 (4.9)	−2.3	35.0 (3.2)	−0.2	54.5 (3.9)	−1.4
Snow depth (cm)						
Fall	23.8 (1.6)	−0.4	11.9 (3.4)	−0.2	25.7 (1.6)	0.2
Winter	29.8 (3.4)	−1.0	22.1 (3.1)	−0.3	33.7 (2.9)	−0.2
Ice thickness (m)						
Fall	2.6 (0.3)	−0.20	1.4 (0.1)	−0.04	2.7 (0.3)	−0.19
Winter	2.9 (0.3)	−0.17	2.1 (0.2)	−0.01	3.2 (0.3)	−0.13
Ice volume (km^3)						
Fall	13021 (2280)	−1237	4014 (668)	33	9006 (2213)	−1269
Winter	16420 (1562)	−862	7863 (1258)	751	8557 (2690)	−613

[a]Quantities within parentheses are the standard deviations of the 5-year means.

discussion of the seasonal consistency of the freeboards and snow depths. Tables 2 and 3 show that, between the fall and winter, there is an overall increase in mean freeboard and snow depth. The increases are higher in regions with more extensive FY ice coverage. This larger increase in freeboard is due to the higher growth rates of thinner FY ice with a thinner snow cover compared to the thicker MY ice. The mean snow depth over FY ice in the fall (11.9 (3.4) cm) is less than half of that over MY ice (25.7 (1.6) cm). Snow depth on FY ice is dependent on the timing of the advance of the seasonal ice cover during the fall. The mean increase in snow depth between fall and winter on FY and MY ice (<10 cm) is only a fraction of the total snow depth because of the rapid buildup of the snow cover in September and October [e.g., *Warren et al.*, 1999; *Sturm et al.*, 2002] due to early winter storms prior to the fall ICESat campaigns. It is also interesting to note that the variability in the mean snow depth over the 5 years (Table 2) is only several centimeters: consistent with the interannual variability during the fall and winter of 3–5 cm reported by *Warren et al.* [1999].

[31] The spatial patterns of ice thickness and their distributions for the 10 ICESat campaigns are shown in Figure 6. These maps of ice thickness are on a 25-km grid. The thickness of each grid element represents the mean thickness of all 25-km ICESat segments that fall inside the grid boundaries within each campaign. Only 25-km segments that contain sea surface estimates (tie points) are used in the construction of these thickness maps. Broadly, all the thickness fields show a distinct transition in thickness between the seasonal and perennial ice zones. This is especially pronounced in the fall. Also, the gradient in the spatial fields across the Arctic follow a distinctive pattern with the thickest multiyear ice (5–6 m) next to Ellesmere Island and the Greenland Coast, followed by a gradual thinning toward the central Arctic and coast of Siberia. The seasonal increase in ice thickness (purple to blue) is most evident in the FY zone.

[32] The 5-year mean ice thickness during the winter is 2.9 (0.3) m, with mean winter thicknesses of 3.2 (0.3) m and 2.1 (0.2) m in the MY and FY ice zones. The behavior of the fall ice thickness can be found in Table 2. The average increase in ice thickness between the fall and winter (Table 3) in the MY and FY zones is 0.5 m and 0.7 m. In interpreting these numbers, it is important to remember that these mean thicknesses represent the mean of the thickness distributions and so they include the effects of deformation (opening and closing). That is, changes in thickness reflect both the thermodynamic (ice growth) and dynamic (ridging) modifications to the thickness distribution. While a change in ice thickness during the winter is an indicator of growth, it also includes thickening (more likely in the winter) and thinning associated with mechanical redistribution. The uncertainties in the mean thickness values are small because the population in each category is large. If we take the uncertainty of each 25-km ICESat segment to be ~0.5 m (from section 3) then the uncertainty over the entire Arctic ice cover is $\frac{0.5}{\sqrt{N}}$ m, where N is the number of samples in the population. There are ~11,000 25-km grid samples within the Arctic Ocean, thus the uncertainty in the population mean is less than several percent of the sample uncertainty of 0.5 m. Of course, this assumes the thickness estimates are unbiased. For a treatment of the sources of error and how they might affect our thickness estimates, the reader is referred to KC08.

[33] Figure 6 also shows the thickness distributions of the entire ice cover and of the MY and FY ice zones. They are constructed from individual ICESat footprints instead of the gridded 25-km means of the spatial fields. Qualitatively, the seasonal changes in the distributions associated with ice growth and deformation can be seen. Compared to the distributions from the FY ice zones, we see fairly long tails in the overall and MY thickness distributions that are most likely from the thicker/older ice cover adjacent to

Table 3. Mean Seasonal Changes in Sea Ice Freeboard, Snow Depth, Thickness, and Volume Between the Fall And Winter ICESat Campaigns[a]

	Overall	FY	MY
Ice freeboard (cm)	5.7	12.5	9.0
Snow depth (cm)	6.0	10.2	7.9
Ice thickness (m)	0.3	0.7	0.5
Ice volume (km^3)	3400	3849	−449

[a]With a larger percentage of first-year ice coverage in the winter, the mean winter ice freeboard and thickness are lowered; thus, the overall seasonal changes are less than either the FY or MY seasonal changes.

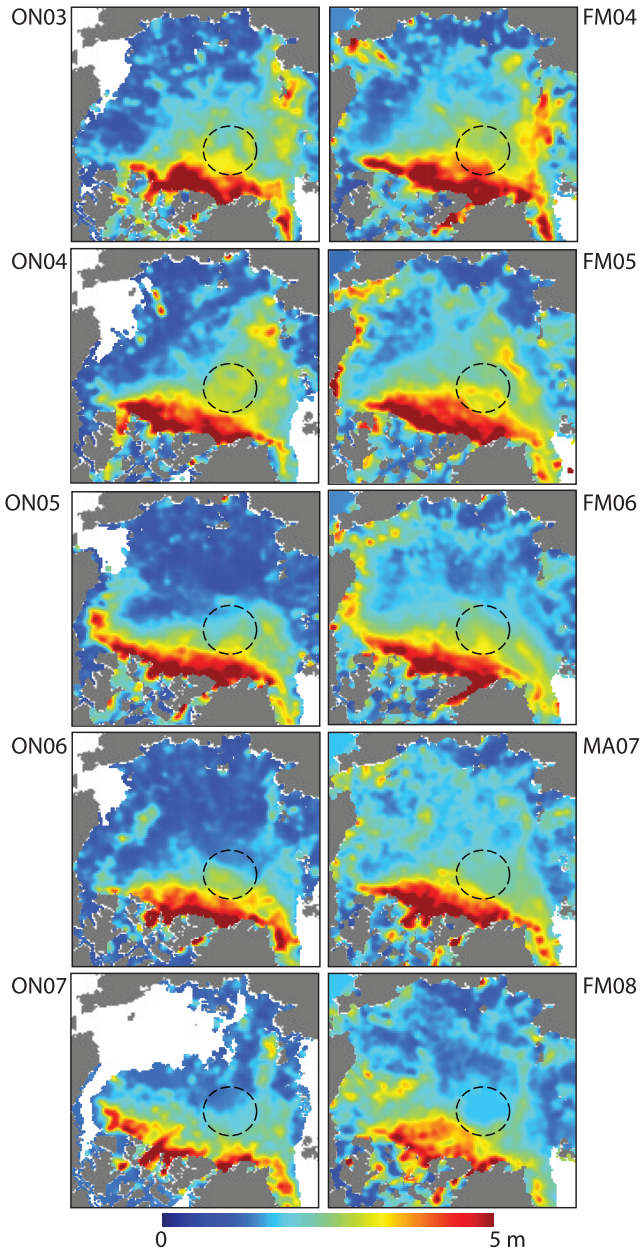

Figure 7. Spatial pattern of sea ice thickness (same as Figure 6) except with the satellite hole filled, with a different color palette to emphasize the ice cover with thicknesses >2.5 m, and smoothed with a 50-km Gaussian kernel. The dashed circle shows the ICESat data hole.

coastal Greenland, in the Lincoln Sea, and the Canadian Archipelago.

5.2. Sea Ice Volume

[34] For examining the interannual and seasonal variability of ice volume, we first fill the data gaps in our gridded field of ice thickness, especially the data hole around the North Pole. Even though the hole in ICESat coverage occupies only ~7% of the area of the Arctic Ocean, it is important to have a reasonable estimate of the ice thickness inside the hole so as to minimize the effects due to advection and the variable coverage of MY and FY ice on the estimates of total Arctic Ocean ice volume. In recent years, this area contains a mixture of FY and MY ice (see Figure 5d) rather than predominantly MY ice. To fill the hole and data gaps, we follow the procedure outlined in KC08. For each missing grid point, the QuikSCAT MY ice fraction at that location is used to provide an estimate of the mean thickness using corresponding samples of MY ice fraction and thickness in the local neighborhood. The QuikSCAT data have a negligible hole around the pole. The local MY fraction is assumed to provide a reasonable proxy of the local average ice thickness. This procedure introduces additional uncertainty in the estimates of total volume. The filled ice thickness fields are shown in Figure 7. Ice volume within a grid cell is simply the product of the mean cell thickness (h) and the cell area (A_c). Total volume is the sum over all ice-covered grid cells and its uncertainty can be written as,

$$\sigma_T = N^{1/2}\left(A_c^2\sigma_h^2 + h^2\sigma_{A_c}^2\right)^{1/2} \quad (5)$$

where σ_h and σ_{A_c} are the uncertainties in cell thickness and cell area, and N is the number of grid cells in the population, respectively. Assuming σ_h = 0.5 m, A_c = 625 km^2, and N = 11000, the first term in the above equation ($\sigma_h A_c\sqrt{N}$) is ~33 km^3. The contribution due to uncertainties in ice thickness is very small indeed and should certainly be regarded as the best case. For instance, if the thickness estimates were biased by e_h, the volume estimate would be biased by $e_h A_{cell}N$. In effect, this is quite tolerant of random errors because of the expected magnitude of the total ice volume. The second term deserves some attention. In winter, when our Arctic domain is fixed and filled with ice, there is no uncertainty in ice extent except for uncertainties in the location of coastal boundaries. During the fall, however, we use passive microwave ice concentration fields to compute ice extent and there could be uncertainties in ice coverage at the ice edge. This source of error could be up to several percent of the total volume, and is dependent on the ice thickness (typically thinner) at the ice edge.

[35] With the above procedure, we obtain the following ice volumes inside the finite area of the Arctic Ocean. Over the 5-year record, the mean Arctic Ocean ice volume is 13021 (2280) km^3 and 16420 (1562) km^3 in the fall and the winter. In winter, the mean ice volume in the seasonal ice zone, 7863(1258) km^3, is nearly as large as the mean volume (8557 (2690) km^3) stored in the MY ice zone. Mean ice production, less ice export, during the ~4.5 months of the winter is 3400 km^3, or equivalently ~0.47 m of sea ice. While there is an increase in mean ice volume in the FY ice zone (3849 km^3) between fall and winter, there is a decrease in mean ice volume in the MY ice zone (−449 km^3). These results seem to indicate that even though there is an increase in the mean thickness in the MY ice zone associated with ice growth and deformation, there is a loss of volume that could be attributed to the export of thick MY ice through the Fram Strait and other passages into the peripheral seas. Because of the large decline in MY coverage in this short 5-year record (Figure 5e), mean volume export exceeds that of ice volume production over a reduced MY ice area. A rough compar-

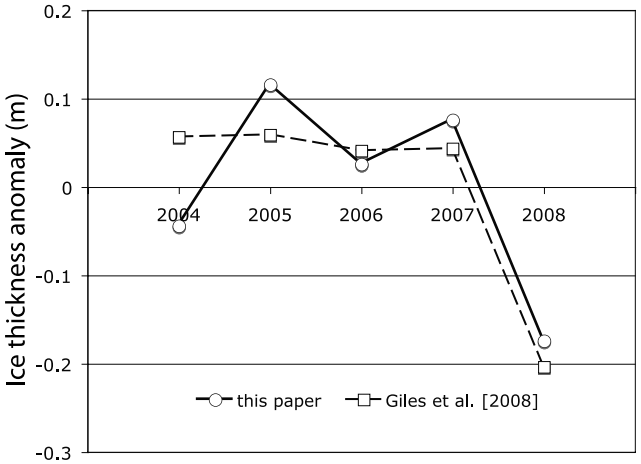

Figure 8. Comparison of 5 years of winter Arctic sea ice thickness anomalies (this paper) with those reported by *Giles et al.* [2008]. Anomalies are calculated for that part of the Arctic Ocean below 81.5°N. Thickness anomalies from Envisat satellite radar altimetry are provided by K. Giles (Center for Polar Observation and Modeling).

ison of our growth and production estimates with those in the published literature can be found in KC08.

6. Trends in Ice Area, Thickness, and Volume: 2003–2008

[36] This short ICESat record (2003–2007) shows thinning of the Arctic ice cover that is coincident with declines in MY ice coverage, resulting in a significant loss in total ice volume. The negative trends in these quantities can be seen in Figure 5 and their numerical values are listed in Table 2. In the following, we restrict our discussion to the observed changes and trends within the ice cover.

[37] Together with the changes in the Arctic Ocean thickness, we find the trends in MY coverage from QuikSCAT [*Kwok*, 2005] to be very useful for understanding and diagnosing the changes and variability in total sea ice volume within the Arctic Basin. The negative trend of -324×10^3 km^2/a in winter MY (1 January) coverage is large and significant (Figure 5e). The precipitous losses came in the years following the small increase in coverage during the winter of 2005. Between 2004 and 2008, there was a net decrease of 1540×10^3 km^2 in MY ice area – a 42% reduction in total MY coverage. Instead of covering just over half (50%) of the Arctic Ocean during the winter of 2004, multiyear ice covered only a third (~34%) of that area in 2008. As a result, seasonal ice became the dominant ice type in the Arctic Basin.

[38] The trends in overall ice thickness (including the MY and FY ice zones) are negative and similar during the fall and winter (−0.2 m/a). More interestingly, Table 2 and Figure 5c show that the trends in the FY zone are negligible and the observed trends are due almost entirely to thinning of the sea ice cover in the MY ice zone. At the beginning of the ICESat record, the mean ice thickness in the MY ice zone was 3.0/3.4 m in the fall/winter. These mean thicknesses fell to 2.3/2.8 m by the end of the record – a net thinning of ~0.6 m of the older ice in the Arctic Ocean. At the same time, the mean thickness of the FY ice zone remained at 1.4/2.1 m during the fall/winter. It seems noteworthy that the delayed formation of the seasonal ice cover after the record summer minimum of 2007 had very little impact on seasonal ice growth/production. The thinner snow depth during that growth season suggests that higher ice production was due in part to reduced accumulation of that large fraction of snowfall that typically occurs in October and November (resulting in lower insulation). Overall, our estimates of the decline in thickness (below 81.5°N) agree remarkably well (Figure 8) with the Envisat-derived thickness anomalies reported in *Giles et al.* [2008]: they are within 0.1 m of each other. Moreover, they show the same dramatic decline in thickness between 2007 and 2008.

[39] The trend in ice volume is −1237/−862 km^3/a (fall/winter). On the whole, the changes in volume represent a net loss of 5400/3500 km^3 (in the fall/winter) during the ICESat record. In terms of percentage loss relative to the mean volume in 2003/04 (Table 2), they are 42% and 21% for the fall and winter. This seasonal contrast in the volume losses is high: the larger volume loss during the fall is likely due to the later formation of the seasonal ice cover associated with the record minimums in summer ice coverage in recent years. Partitioning the volume changes between the FY and MY ice zones provides another view of the changes in the ice cover. The loss in MY ice volume is larger than the overall ice volume loss (Figure 5f). As seen in Figure 5f and Table 2, the large negative trend in MY sea ice volume is only partially compensated by the positive trend in the FY sea ice volume. At the end of the record, the volume stored in MY ice during the winter (4500 km^3 or 32% of total volume) has become lower than that stored in FY ice zone (9400 km^3; 68% of total volume). This can be compared to the beginning of the record when the winter MY volume at 10800 km^3 (62% of total volume) is larger than that stored in FY ice (6600 km^3 or 38%). Over this short record, there is a near reversal in the volumetric contribution of the two ice types to the total volume of the Arctic Ocean ice cover.

[40] To summarize, the ICESat record shows a clear decrease in overall ice thickness and loss of ice volume of the Arctic Ocean ice cover. The simultaneous decline in MY coverage and the thinning of the MY ice in recent years have had considerable impact on the total volume of the ice cover. The reversal in the coverage and volume of the MY and FY is remarkable over this 5 short years. Seasonal ice, having surpassed that of MY ice in winter area coverage and volume, became the dominant ice type at the end of the record.

7. Loss of MY Ice Area/Volume and Summer Replenishment

[41] On the basis of the above discussion, the primary changes in the overall thickness and volume of the Arctic Ocean sea ice are attributable to the thinning of the MY ice cover and the decline in MY ice coverage. Over the winter record, there is a net loss of 57% of MY sea volume (6300 km^3) and a 42% reduction in MY coverage relative to their values in the winter of 2004. At the same time, the thickness of the FY ice cover has not changed significantly.

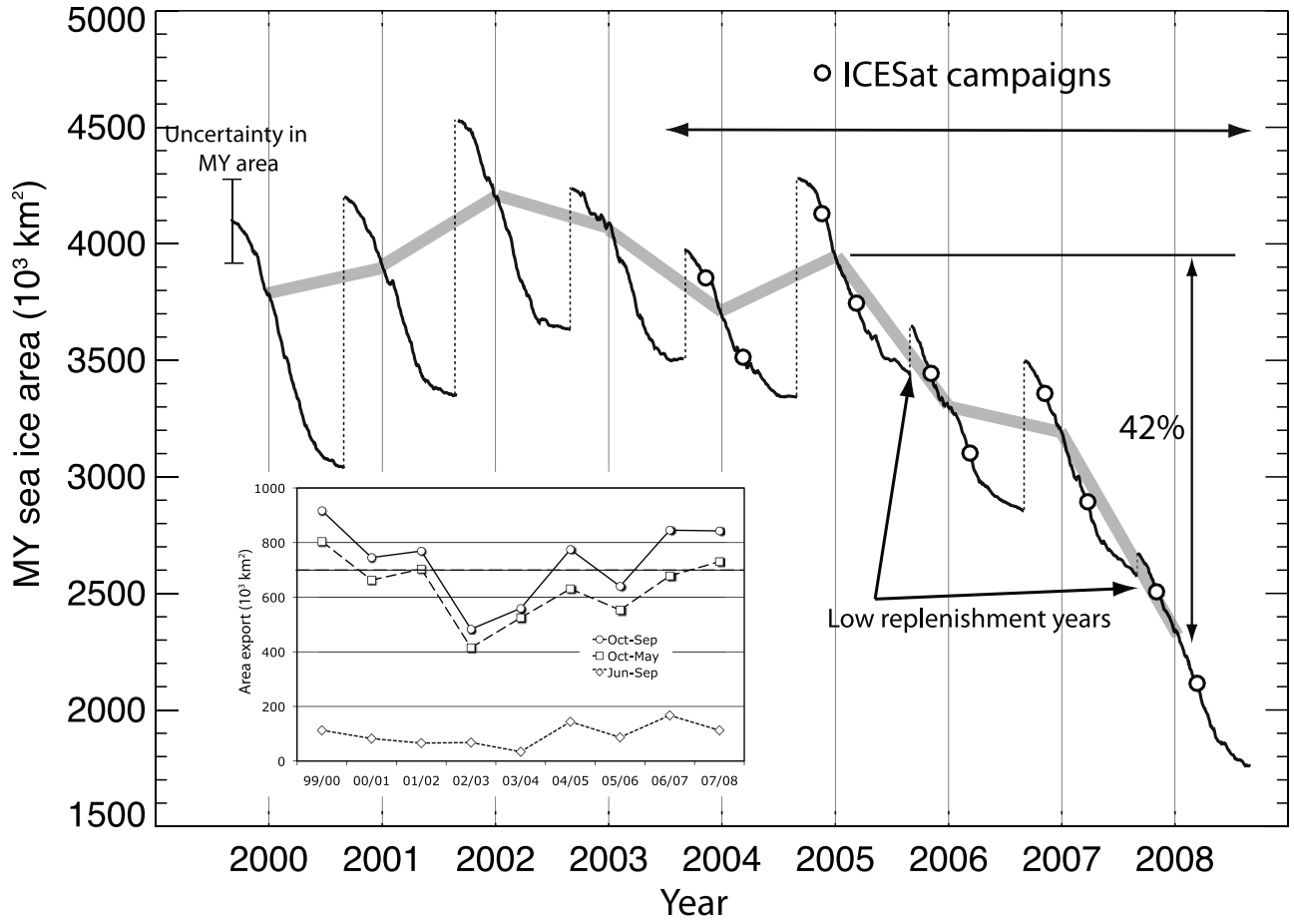

Figure 9. Nine annual cycles of replenishment/export of Arctic Ocean multiyear ice area constructed using QuikSCAT data and Fram Strait ice export. Open circles show the approximate times of the 10 ICESat campaigns used here. The dashed vertical lines show the replenishment of the MY ice reservoir by first-year ice at the end of each summer. The two near-zero replenishment years of 2005 and 2007 are indicated. Inset shows the annual and seasonal Fram Strait ice export over the same period.

Here, we examine the changes in the MY ice cover from the perspective of replenishment, export, and melt.

[42] The annual cycles of MY ice coverage since 1999, constructed using the procedures by *Kwok* [2007], are shown in Figure 9. Seasonally, the MY ice area shows a monotonic decrease in coverage from the beginning of the growth season (late September) that is due to ice export primarily through the Fram Strait. On average, ~10% of the Arctic Ocean ice cover is lost to export every year. Sea ice outflow is typically lower during the summer months (June–September) because of the weaker sea level pressure gradients across the strait. Also, there is lower MY fraction at the fluxgate during the summer. That area of FY ice that survives the summer contributes the step increase in MY ice area at the end of each summer. These FY ice areas replenish the Arctic Ocean MY ice reservoir after each year's depletion through export and melt. Balance between export, melt, and replenishment is necessary to maintain a stable MY ice area.

[43] Up through the summer of 2005, the annual replenishment was sufficient to maintain a relatively stable MY ice coverage of $\sim 4 \times 10^6$ km^2 (Figure 9) although the variability was remarkably high. For example, there was over a million square kilometers of replenishment at the end of the summers of 2000 and 2001. In the shorter record (2000–2006) reported by *Kwok* [2007], the near-zero replenishment at the end of summer of 2005 stands out as being the lowest of the six summers. Because of the low replenishment, the MY ice coverage in January 2006 was lower by $\sim 600 \times 10^3$ km^2 when compared to that in January 2005 and is the lowest compared to earlier years. In the longer record shown in Figure 9, the 2007 ice replenishment was the lowest after the record minimum in ice extent that summer and helps set the record on lowest MY coverage. The 2 years (2005 and 2007) of near-zero replenishment seem to have contributed to the dramatic decrease in the Arctic Ocean MY area.

[44] What is the relative role of melt and ice export in these low replenishment years? Could increase in ice export alone explain the net decrease of 1540×10^3 km^2 in MY ice area in 4 years? The inset in Figure 9 shows the net ice export record through the Fram Strait since 2000 reported by *Kwok* [2009]. Over the 9 years, the average net area flux through the Fram Strait of $\sim 730 \times 10^3$ km^2 is not remarkable compared to the 29-year record average of ~ 700 (130) $\times 10^3$ km^2 [*Kwok*, 2009]. In the absence of replenishment of the $\sim 4000 \times 10^3$ km^2 of MY ice in the Arctic prior to 2005, it would take only several years, at an

average export rate, to export all of the MY year ice through the Fram Strait. In fact, increase in ice export is not necessary but would certainly enhance the depletion of MY ice coverage. Of course, this assumes availability of MY ice for export at the Strait and favorable circulation patterns in the Arctic Ocean. In the years shown in Figure 9 (inset), there is a positive trend in Fram Strait export starting in 2003 but, as mentioned above, the export is within the expected variance. In fact, the export is lower than average early in the record and only slightly higher during the last 2 years. So, it seems clear from Figure 9 that the areal melt of FY ice during the summer, rather than export, played a significant role in the depletion of the FY ice area necessary for the replenishment of the MY ice cover.

[45] It is also interesting to note that the small positive trend in summer ice export is unusual over the 29-year record and is associated with changes in large-scale sea ice circulation [*Kwok*, 2009]. The consequence of summer ice export is different from that of the winter and deserves some attention. During the winter or growth season, the MY ice area in the Arctic Ocean depleted by area export is replaced by FY ice. Depending on the winter conditions, these seasonal ice areas have an opportunity to grow and thus a chance to survive the subsequent summer and contribute to the replenishment of the MY ice reservoir. This is not true of ice area exported during the summer. Since there is no freezing of the vacated areas, summer export contributes directly to the depletion of the following fall's MY ice cover and to open water production. From the replenishment perspective, for a given net annual ice export it would be better to have higher ice export during the early winter than the summer.

[46] The thinning of the MY ice is more difficult to address and could be due to a number of factors: ice age, export, and melt. The negative trend in MY thickness together with the spatial field in Figure 6 shows a thinner MY ice cover especially in that region of the ice cover between the Greenland coast and the North Pole. This could perhaps be due to a younger MY ice pack as suggested by *Rigor and Wallace* [2004] and *Maslanik et al.* [2007]. Thicker/older MY ice could be exported though the Nares Strait as well [*Kwok*, 2005]. In terms of melt, *Perovich et al.* [2008] report that there was an extraordinarily large amount of melting on the bottom of the ice in the Beaufort Sea in the summer of 2007. However, their North Pole buoy exhibited bottom and surface melt that is similar to previous years. This thinning of the MY ice cover begs further investigation.

8. Summary

[47] In this paper, we present our best estimate of the thickness and volume of the Arctic Ocean ice cover from 10 ICESat campaigns (October 2003 through March 2008) and examine the large-scale changes of the ice cover based on these 5 years. To assess the quality of our estimates, we compare the thickness data with available ice draft profiles. At a 25-km length scale, results show that ice drafts are consistently within 0.5 m (standard deviation) of profiles from a submarine cruise in mid-November of 2005, and 4 years of ice draft from moorings in the Chukchi and Beaufort seas. Guided by this assessment of the thickness estimates and assuming that the errors are random and unbiased, the uncertainties in Arctic ice thicknesses and volumes discussed below are less than several percent of the population mean. In the remainder of this section, we summarize the noteworthy results from different parts of the paper.

[48] Seasonally, the 5-year mean ice thickness during the winter is 2.9 (0.3) m, with mean winter thicknesses of 3.2 (0.3) m and 2.1 (0.2) m in the MY and FY ice zones. In the ~4.5-month interval between the fall and winter, the average increase in ice thickness in the MY and FY zones is 0.5 m and 0.7 m. These seasonal increases include ice growth/melt and the effects of deformation (opening and closing) and are an expression of both the thermodynamic and dynamic modifications to the thickness distribution. Over the record, the trends in overall ice thickness (including the MY and FY ice zones) are negative and similar during the fall and winter (−0.2 m/a). The trends in the FY zone are negligible and the observed trends are due almost entirely to thinning of the sea ice cover in the MY ice zone. At the beginning of the ICESat record, the mean ice thickness in the MY ice zone was 3.0/3.4 m in the fall/winter. These mean thicknesses fell to 2.3/2.8 m by the end of the record – a net thinning of ~0.6 m of the older ice in the Arctic Ocean. At the same time, the mean thickness of the FY ice zone remained at 1.4/2.1 m during the fall/winter.

[49] The mean Arctic Ocean ice volume is 13021 (2280) km^3 and 16420 (1562) km^3 in the fall and the winter. In winter, the mean ice volume in the seasonal ice zone, 7863 (1258) km^3, is nearly as large as the mean volume (8557 (2690) km^3) stored in the MY ice zone. Net ice production (production minus export) during the ~4.5 months of the winter is 3400 km^3, or equivalently ~0.47 m of sea ice. The 5-year trends in ice volume are −1237 and −862 km^3/a during the fall and winter, respectively. On the whole, there is a net loss of 5400/3500 km^3 (in the fall/winter) between the beginning and end of this record. In terms of percentage loss relative to the mean volume in 2003/04, they are 42% and 21% for the fall and winter. Ice volume loss in the MY ice zone is larger than the loss in overall ice volume. The larger negative trend in MY sea ice volume is only partially compensated by the positive trend in the FY sea ice volume (as its coverage increases). At the end of the record, the volume stored in MY ice during the winter (4500 km^3 or 32% of total volume) is lower than that stored in FY ice zone (9400 km^3; 68% of total volume). Compared to the beginning of the record, the winter MY volume at 10800 km^3 (62% of total volume) was larger than that stored in FY ice (6600 km^3 or 38%). At the same time, the negative trend of -324×10^3 km^2/a in winter MY (1 January) coverage is large and significant. Between 2004 and 2008, there was a net decrease of 1540×10^3 km^2 in MY ice area – a 42% reduction in total MY coverage. Instead of covering just over half (50%) of the Arctic Ocean in 2003, multiyear ice covered only a third (~34%) of that area during the winter of 2008.

[50] To sum up, the primary changes in the overall thickness and volume of the Arctic Ocean sea ice are attributable to the thinning of the MY ice cover and the decline in MY ice coverage. Over the winter record, there is a net loss of 57% of MY sea volume (6300 km^3) and a 33% reduction in MY coverage of the Arctic Ocean relative to their values in winter of 2004. These are dramatic changes. At the same time, the thickness of the FY ice cover has not

changed significantly. Over this short record, there is a reversal in the volumetric and areal contributions of the two ice types to the total volume and area of the Arctic Ocean ice cover. Examining the ice export together with the decline in MY ice coverage suggest that the near-zero replenishment of the MY ice cover, an imbalance in the cycle of replenishment and ice export after the summers of 2005 and 2007, has played a significant role in the loss of Arctic sea ice volume over the ICESat record. Changes in MY ice export, by itself, do not explain the record minimums in recent years.

[51] This represents a broad examination of the basin-scale changes that have occurred in the Arctic Ocean sea ice thickness and volume over the short ICESat record. The derived seasonal and interannual changes seem reasonably consistent and well constrained. A more detailed evaluation of the regional variability in thickness and volume should be done. These ICESat observations should be placed in the context of the historical record of spatial, annual, and interannual variability of Arctic ice thickness documented in by *Rothrock et al.* [2008]. Like other altimeter missions, there will no doubt be improvements in the ICESat retrievals in the future. Considering the current decline in the Arctic Ocean ice cover, it is unfortunate that there will be a gap in the laser altimeter coverage of the Arctic Ocean due to the lifespan of the current lasers. At the earliest, the planned ICESat-II will be launched in 2014.

[52] **Acknowledgments.** We wish to thank R. Krishfield (WHOI) and H. Melling (IOS) for providing the ice draft profiles from the BGEP and AIM sites, respectively. The AMSR-E brightness temperature and ice concentration fields are provided by World Data Center for Glaciology/National Snow and Ice Data Center, University of Colorado, Boulder, Colorado. ICESat data are from the ICESat Science Team Computing Facility and NSIDC. M.W. and I.R. are funded by a NASA grant. J.Z. and D.Y. are supported by NASA's funding of the ICESat/GLAS Science Team. R.K. carried out this work at the Jet Propulsion Laboratory, California Institute of Technology, under contract with NASA.

References

Comiso, J. C., C. L. Parkinson, R. Gersten, and L. Stock (2008), Accelerated decline in the Arctic sea ice cover, *Geophys. Res. Lett.*, *35*, L01703, doi:10.1029/2007GL031972.

Forsberg, R., and H. Skourup (2005), Arctic Ocean gravity, geoid and seaice freeboard heights from ICESat and GRACE, *Geophys. Res. Lett.*, *32*, L21502, doi:10.1029/2005GL023711.

Giles, K. A., S. W. Laxon, and A. L. Ridout (2008), Circumpolar thinning of Arctic sea ice following the 2007 record ice extent minimum, *Geophys. Res. Lett.*, *35*, L22502, doi:10.1029/2008GL035710.

Kwok, R. (2004), Annual cycles of multiyear sea ice coverage of the Arctic Ocean: 1999–2003, *J. Geophys. Res.*, *109*, C11004, doi:10.1029/2003JC002238.

Kwok, R. (2005), Variability of Nares Strait ice flux, *Geophys. Res. Lett.*, *32*, L24502, doi:10.1029/2005GL024768.

Kwok, R. (2007), Near-zero replenishment of the Arctic multiyear sea ice cover at the end of 2005 summer, *Geophys. Res. Lett.*, *34*, L05501, doi:10.1029/2006GL028737.

Kwok, R. (2009), Outflow of Arctic sea ice into the Greenland and Barents seas: 1979–2007, *J. Clim.*, *22*, 2438–2457, doi:10.1175/2008JCLI2819.1.

Kwok, R., and G. F. Cunningham (2008), ICESat over Arctic sea ice: Estimation of snow depth and ice thickness, *J. Geophys. Res.*, *113*, C08010, doi:10.1029/2008JC004753.

Kwok, R., A. Schweiger, D. A. Rothrock, S. Pang, and C. Kottmeier (1998), Sea ice motion from satellite passive microwave data assessed with ERS SAR and buoy data, *J. Geophys. Res.*, *103*, 8191–8214.

Kwok, R., H. J. Zwally, and D. Yi (2004), ICESat observations of Arctic sea ice: A first look, *Geophys. Res. Lett.*, *31*, L16401, doi:10.1029/2004GL020309.

Kwok, R., G. F. Cunningham, H. J. Zwally, and D. Yi (2006), ICESat over Arctic sea ice: Interpretation of altimetric and reflectivity profiles, *J. Geophys. Res.*, *111*, C06006, doi:10.1029/2005JC003175.

Kwok, R., G. F. Cunningham, H. J. Zwally, and D. Yi (2007), Ice, Cloud, and land Elevation Satellite (ICESat) over Arctic sea ice: Retrieval of freeboard, *J. Geophys. Res.*, *112*, C12013, doi:10.1029/2006JC003978.

Maslanik, J. A., C. Fowler, J. Stroeve, S. Drobot, J. Zwally, D. Yi, and W. Emery (2007), A younger, thinner Arctic ice cover: Increased potential for rapid, extensive sea ice loss, *Geophys. Res. Lett.*, *34*, L24501, doi:10.1029/2007GL032043.

Melling, H., P. H. Johnston, and D. A. Riedel (1995), Measurement of the topography of sea ice by moored sub-sea sonar, *J. Atmos. Oceanic Technol.*, *12*, 589–602, doi:10.1175/1520-0426(1995)012<0589:MOTUTO>2.0.CO;2.

National Snow and Ice Data Center (2006), Submarine upward looking sonar ice draft profile data and statistics, http://nsidc.org/data/g01360.html, Boulder, Colo.

Perovich, D. K., J. A. Richter-Menge, K. F. Jones, and B. Light (2008), Sunlight, water, and ice: Extreme Arctic sea ice melt during the summer of 2007, *Geophys. Res. Lett.*, *35*, L11501, doi:10.1029/2008GL034007.

Polyakov, I., et al. (2007), Observational program tracks Arctic Ocean transition to a warmer state, *Eos Trans. AGU*, *88*(40), 398–399, doi:10.1029/2007EO400002.

Proshutinsky, A., R. Krishfield, E. Carmack, F. McLaughlin, S. Zimmerman, K. Shimada, and M. Itoh (2004), Annual freshwater and heat content from 2003–2004: First results from the Beaufort Gyre observing system, *Eos Trans. AGU*, *85*(47), Fall Meet. Suppl., Abstract C41A-0182.

Rigor, I. G., and J. M. Wallace (2004), Variations in the age of Arctic sea ice and summer sea ice extent, *Geophys. Res. Lett.*, *31*, L09401, doi:10.1029/2004GL019492.

Rothrock, D. A., and M. Wensnahan (2007), The accuracy of sea ice drafts measured from U.S. Navy submarines, *J. Atmos. Oceanic Technol.*, *24*, 1936–1949, doi:10.1175/JTECH2097.1.

Rothrock, D., D. B. Percival, and M. Wensnahan (2008), The decline in Arctic sea ice thickness: Separating the spatial, annual, and interannual variability in a quarter century of submarine data, *J. Geophys. Res.*, *113*, C05003, doi:10.1029/2007JC004252.

Schwarz, J., and W. F. Weeks (1977), Engineering properties of sea ice, *J. Glaciol.*, *19*(81), 499–530.

Stroeve, J., et al. (2008), Arctic sea ice extent plummets in 2007, *Eos Trans. AGU*, *89*(2), 13, doi:10.1029/2008EO020001.

Sturm, M., J. Holmgren, and D. K. Perovich (2002), Winter snow cover on the sea ice of the Arctic Ocean at the Surface Heat Budget of the Arctic Ocean (SHEBA): Temporal evolution and spatial variability, *J. Geophys. Res.*, *107*(C10), 8047, doi:10.1029/2000JC000400.

Warren, S. G., I. G. Rigor, N. Untersteiner, V. F. Radionov, N. N. Bryazgin, Y. I. Aleksandrov, and R. Colony (1999), Snow depth on Arctic sea ice, *J. Clim.*, *12*, 1814–1829.

Weeks, W. F., and O. S. Lee (1958), Observation on the physical properties of sea ice at Hopedale, Labrador, *Arctic*, *11*(3), 134–155.

Wensnahan, M., and D. A. Rothrock (2005), Sea ice draft from submarine-based sonar: Establishing a consistent record from analog and digitally recorded data, *Geophys. Res. Lett.*, *32*, L11502, doi:10.1029/2005GL022507.

Woodgate, R. A., K. Aagaard, and T. J. Weingartner (2006), Interannual changes in the Bering Strait fluxes of volume, heat and freshwater between 1991 and 2004, *Geophys. Res. Lett.*, *33*, L15609, doi:10.1029/2006GL026931.

Zwally, H. J., et al. (2002), ICESat's laser measurements of polar ice, atmosphere, ocean, and land, *J. Geodyn.*, *34*, 405–445, doi:10.1016/S0264-3707(02)00042-X.

Zwally, H. J., D. Yi, R. Kwok, and Y. Zhao (2008), ICESat measurements of sea ice freeboard and estimates of sea ice thickness in the Weddell Sea, *J. Geophys. Res.*, *113*, C02S15, doi:10.1029/2007JC004284.

G. F. Cunningham and R. Kwok, Jet Propulsion Laboratory, California Institute of Technology, 4800 Oak Grove Drive, Pasadena, CA 91109, USA. (ron.kwok@jpl.nasa.gov)

I. Rigor and M. Wensnahan, Polar Science Center, Applied Physics Laboratory, University of Washington, 1013 NE 40th Street, Seattle, WA 98105, USA.

D. Yi, SGT, Inc., NASA Goddard Space Flight Center, Code 614.1, Greenbelt, MD 20771, USA.

H. J. Zwally, Cryospheric Sciences Branch, Code 614.1, NASA Goddard Space Flight Center, Greenbelt, MD 20771, USA.